

ARTICLE OPEN



Charge transfer induced symmetry breaking in GaN/Bi₂Se₃ topological heterostructure device

Faizan Ahmad¹, Rachana Kumar² , Sunil Singh Kushvaha², Mahesh Kumar²  and Pramod Kumar¹ 

In topological insulators (TI) for surface electron transport, dissipationless surface states are required and are activated by symmetry breaking usually by reducing thickness of the film. Substrates play an important role in modulating the surface properties by modifying the surface electronic and mechanical properties. In the present work, we have studied the n-GaN/p-Bi₂Se₃ topological heterojunction for the topological surface states and analyzed by Raman and ultrafast transient absorption (TA) spectroscopy probed in visible and NIR regions. Raman spectrum clearly shows the electron-phonon interaction at the surface by appearance of surface phonon modes (SPM) in heterojunction. TA spectroscopy is performed on Glass/Bi₂Se₃ and n-GaN/Bi₂Se₃ heterojunction to identify surface states, energy levels, charge transfer and carrier relaxation processes. Electrical measurements under dark and illuminated conditions were performed for deeper understanding of the interface states and their effect on electrical and optical performance. The study provides complete understanding of n-GaN/TI-based interfaces by spectroscopic and electrical measurements for their application in next-generation electronic and optical devices.

npj 2D Materials and Applications (2022)6:12; <https://doi.org/10.1038/s41699-022-00288-7>

INTRODUCTION

Topological insulators (TI) are one of the main classes of electronic material finding applications in next-generation high-speed devices^{1,2}. The two members of this family, i.e., Bi₂Se₃ and Bi₂Te₃ have been studied extensively for their preparation, properties evaluation, and applications in bulk and film forms^{3,4}. The surface states of these materials are topologically protected while bulk is insulating^{5,6}. Efforts were made to effectively enhance the contribution of topological surface states towards conductance by reducing the thickness of the deposited film^{7,8}. The decrease in film thickness causes the symmetry breaking along the z-axis due to loss in infinite crystal periodicity⁹. The symmetry breaking is also dependent on fabrication techniques (even in thick samples) and interaction with substrates (interfaces). It was observed by Wiesner et al.¹⁰, that the substrate interfaces also cause symmetry breaking due to interaction between Bi₂Te₃ and substrates. This makes the surface properties different from that of the from bulk even in samples with thickness ~150 nm^{11,12}. Studies have been reported for the Bi₂Se₃ based heterostructure for surface modulation due to interface effect. There have been reports where Bi₂Se₃ heterostructure are explored as potential photo-detector application^{13–16}.

The surface electronic states in Bi₂Se₃ are gapless and are characterized by a linear dispersion known as Dirac states. Angle-resolved photoemission spectroscopy (ARPES) measurements identify two Dirac cones, consist of occupied (SS1) and unoccupied (SS2) surface states, which are separated by an energy gap of ~1.8 eV¹⁷. The existence of such inter-band transition at the surface provides a way to distinguish optical transitions. The surface excitation of the charge carriers has different charge transfer dynamics from the bulk that is interesting to explore¹⁸. Several spectroscopy methods have been reported to study ultrafast dynamics of generated charge carriers in TI materials. Among them, more studied are transient reflectivity (TR) spectroscopy, TrARPES, SHG, etc. Our group has performed

study on topological material based device optimization for transport and interface dynamics in Si/Bi₂Te₃ and Ge/Bi₂Te₃^{19–21}. Work related to the study of the transport property in p-Si/n-Bi₂Te₂Se heterojunction under illumination has also been recently reported by us²². TR spectroscopy was performed on Bi₂Se₃ nanoflakes at 10 K and 300 K by Jnawali et al.²³ to study the thermalization and recombination dynamics over a wide energy range using 810 nm (1.5 eV) pump wavelength. This pump energy is directly interacting with the second surface state (SS2) at higher energy. Glinka et al.²⁴ studied the ultrafast carrier dynamics by transient absorption (TA) spectroscopy of two-photon excited electron (~3.4 eV) in Bi₂Se₃ film using 730 nm (~1.7 eV) pump wavelength and probing in the visible region. They concluded that the carrier relaxation dynamics are highly influenced by the position of the Dirac point. When the energy gap between the Dirac cones is higher than phonon and resonance defect energy, the relaxation dynamics of the charge carrier are forced to be very slow. They also suggested for mid-IR probe range to study the ultrafast carrier relaxation dynamics in the lowest most Dirac surface states.

High quality Bi₂Se₃ films of low thickness are more commonly prepared by molecular beam epitaxy (MBE) and suffer with high cost and time consuming fabrication process²⁵. In the present work we have fabricated the polycrystalline Bi₂Se₃ film of ~150 nm over n-GaN substrate using cost effective thermal deposition technique. GaN is a direct wide band gap semiconductor material with band gap of 3.4 eV¹⁵ having wurtzite structure [hexagonal, space group P6₃mc (186)] matches well with crystal structure as of Bi₂Se₃ (rhombohedral, space group R-3m (166)) forming well aligned morphology. In this work, we have studied the GaN/Bi₂Se₃ interface contributing to the modulation of topological surface states in the n-GaN/p-Bi₂Se₃ topological heterojunction. To explain the bulk and heterojunction photo-generated carrier dynamics and charge transfer (CT) states formation, we have performed ultrafast femtosecond transient absorption spectroscopy study on

¹Spintronics and Magnetic Materials Laboratory, Department of Applied Sciences, IIIT-Allahabad, Prayagraj 211012, India. ²CSIR- National Physical Laboratory, New Delhi 110012, India. email: rachanak.npl@nic.in; pkumar@iiita.ac.in

Bi_2Se_3 films over a glass and GaN/ Bi_2Se_3 heterojunction using 410 nm (3.024 eV) pump wavelength and probed in both visible and NIR region. The photoelectric effect of n-GaN/p- Bi_2Se_3 heterojunction was studied under the presence of optical light with a varying wavelength. The CT states were further investigated and quantified by the capacitance-voltage (C-V) measurements. The time constant and behavior were probed by conductance/radial frequency- radial frequency ($G_p/\omega-\omega$) plot. The study gives a significant insight and deeper understanding of CT states that are responsible for the topological surface states existence in thick Bi_2Se_3 topological insulator film in n-GaN/p- Bi_2Se_3 heterojunction.

RESULTS AND DISCUSSION

Comparative X-ray diffractogram of Glass/ Bi_2Se_3 and n-GaN/ Bi_2Se_3 with bulk Bi_2Se_3 was studied for the phases of the film grown Bi_2Se_3 TI film (refer. Supplementary Fig. 2). XRD peaks of films confirmed the polycrystalline rhombohedral lattice phase formation. Crystallinity of Bi_2Se_3 film was enhanced after annealing and peaks are shifted towards a lower angle compared to bulk. Glass/ Bi_2Se_3 shows a higher shift compared to n-GaN/ Bi_2Se_3 films due to substrate strain effect and strain coefficient was calculated to be 0.022 and 0.00408 over glass and n-GaN respectively. GaN substrate imposes a lesser local strain than glass due to close crystalline structure to Bi_2Se_3 . The Hall measurement confirmed the charge carrier in the Bi_2Se_3 TI deposited film on a glass substrate to be p-type with charge carrier density $\sim 3.19 \times 10^{19}/\text{cm}^3$ and mobility $\sim 6.16 \text{ cm}^2/\text{V}\cdot\text{s}$ respectively (refer. Supplementary Fig. 3). The values obtained are in good agreement with earlier reported values for the same²⁶. Thickness of the film over glass was ~ 150 nm. Same conditions were used to deposit film over n-GaN substrates. Energy dispersive X-ray spectroscopy (EDS) confirmed the stoichiometry and SEM image confirmed the uniformity of

films (refer. Supplementary Fig. 4a, b. AFM images of Glass/ Bi_2Se_3 and n-GaN/ Bi_2Se_3 are shown (refer. Supplementary Fig. 5). Surface topography of GaN/ Bi_2Se_3 film and GaN/ Bi_2Se_3 film had the root mean square roughness (RMS) of 10 nm and 14 nm respectively (refer. Supplementary Fig. 5).

Raman spectroscopy study

To study the phonon vibrations and electron-phonon interaction in Glass/ Bi_2Se_3 and n-GaN/ Bi_2Se_3 , Raman spectroscopy was performed. As shown in Fig. 1, Raman active bands are visible in both the films. Bi_2Se_3 consists of 5 atoms per unit cell i.e., 15 zone center phonon branches (3 acoustic and 12 optical modes) in phonon dispersion relation. In 12 optical mode phonons, 4 are Raman active and 4 are IR active. Raman spectra show distinct optical phonon modes (A^1_{1g} , E^2_g , A^2_{1g}) as summarized in Table 1. Raman shift and intensity are helpful to identify the quality of the interface. A slight shift of $\sim 2\text{-}3 \text{ cm}^{-1}$ towards lower frequency is observed in the heterostructure. As also inferred in XRD (refer Supplementary Fig. 2), GaN substrate is making a substantial effect on Bi_2Se_3 bond forces resulting in shift towards lower frequency. The peaks are Lorentz fit and data are summarized in Table 1. As can be seen, the full-width half maxima (FWHM) are highly increased in n-GaN/ Bi_2Se_3 films for all the peaks. As also seen in MoS_2/WS_2 heterostructure, the frequency decreases by 2 cm^{-1} due to slightly increased interlayer distance and weaken interlayer coupling²⁷. Raman data of GaN/ Bi_2Se_3 fits well with five peaks (Table 1). Surface phonon mode (SPM) in n-GaN/ Bi_2Se_3 heterojunction is observed at $\sim 95 \text{ cm}^{-1}$ along with the Raman forbidden A^2_{1u} mode at $\sim 162 \text{ cm}^{-1}$. The appearance of A^2_{1u} mode signifies the symmetry breaking of Bi_2Se_3 TI due to interface effect. Similar observation was also reported by Wiesner et al. for $\text{Bi}_2\text{Te}_3/\text{GaAs}$ where A^2_{1u} mode appeared in micro Raman analysis due to substrate effect¹⁰. The symmetry breaking is caused by charge transfer (CT) from n-GaN to p- Bi_2Se_3 . There is effective electron-acoustic phonon coupling in n-GaN/ Bi_2Se_3 heterojunction leading to spin like oscillations of electrons on the surface due to symmetry breaking by substrate at room temperature (refer. Supplementary Figs. 6 and 7)^{28,29}. The ratio of $I(A^2_{1g})/I(E^2_g)$ is increased in n-GaN/ Bi_2Se_3 heterojunction as compared to Glass/ Bi_2Se_3 film suggesting weaker interaction between the layer caused by the effective CT from n-GaN to Bi_2Se_3 which is further confirmed by transient absorption spectroscopy (Table 1).

Transient absorption spectroscopy study

Transient absorption profiles were recorded using 410 nm pump wavelength with a power of 0.2 mW probed in both visible and NIR regions. Probing in the visible region demonstrates charge carrier dynamics in higher energy levels i.e., bulk states (BS) and higher surface state (SS2), whereas, the NIR region probes the charge carrier dynamics in the lower surface states (SS1). Pump is selected below the GaN bandgap and higher than the Bi_2Se_3 bandgap energy. Figure 2 shows the TA spectra of GaN substrate, Glass/ Bi_2Se_3 and GaN/ Bi_2Se_3 in visible and NIR regions. GaN shows strong ground state bleaching (GSB) at 365 nm for the direct band

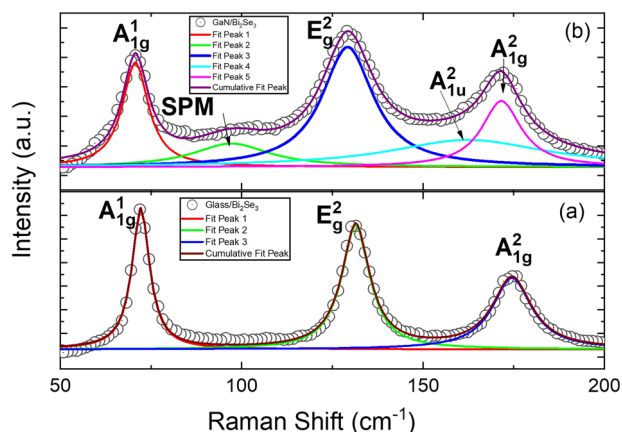


Fig. 1 The Raman spectroscopic results with Lorentz peak fitting. **a** Glass/ Bi_2Se_3 heterojunction, **b** n-GaN/ Bi_2Se_3 heterojunction in the surface phonon mode (SPM).

Vibration mode	Glass/ Bi_2Se_3			n-GaN/ Bi_2Se_3		
	Peak position (cm^{-1})	FWHM (cm^{-1})	$I(A^2_{1g})/I(E^2_g)$	Peak position (cm^{-1})	FWHM (cm^{-1})	$I(A^2_{1g})/I(E^2_g)$
A^1_{1g}	72.19 ± 0.05	5.78 ± 0.14	0.61	70.69 ± 0.18	8.69 ± 0.56	0.69
E^2_g	131.43 ± 0.07	9.13 ± 0.20		129.22 ± 0.24	17.11 ± 0.81	
A^2_{1g}	174.50 ± 0.13	12.42 ± 0.43		171.60 ± 0.30	13.23 ± 1.04	
A^2_{1u}	—	—		162.41 ± 5.21	52.91 ± 12.95	
SPM	—	—		97.16 ± 1.01	37.09 ± 5.71	

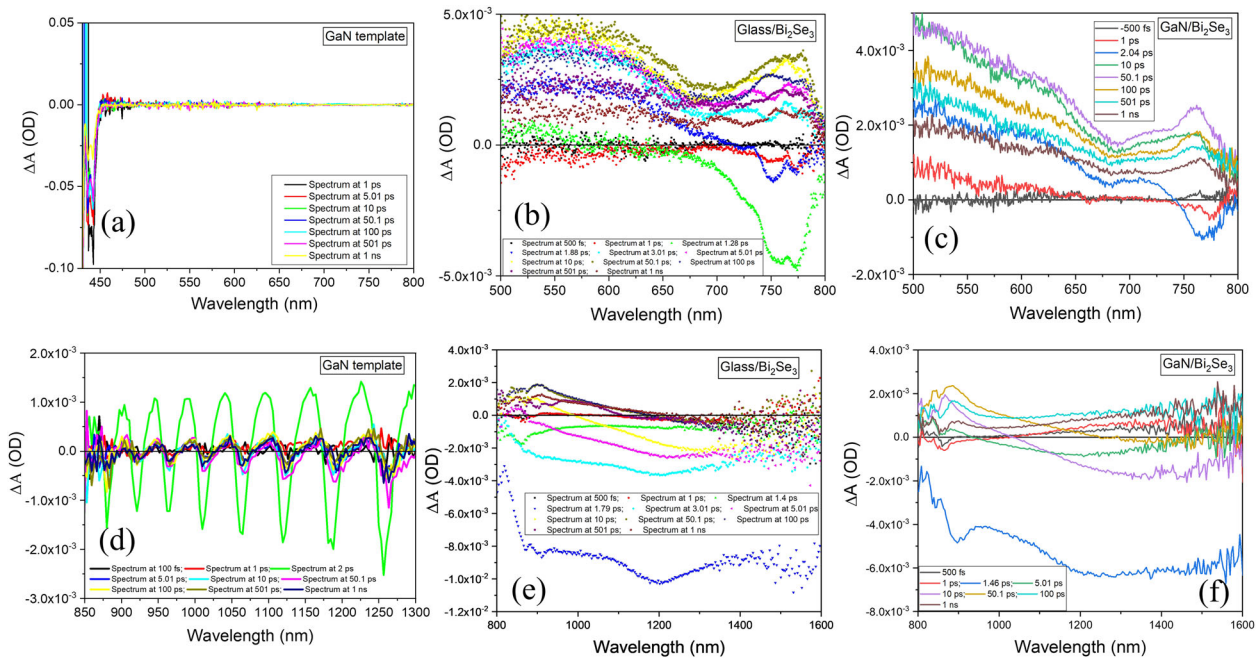


Fig. 2 The transient absorption (TA) spectra results with the amplitude variation (ΔA) vs. wavelength (nm) plot in the visible range (450–800 nm). **a** GaN template, **b** Glass/Bi₂Se₃ heterojunction, **c** n-GaN/Bi₂Se₃ at different time delays. TA spectra with amplitude variation (ΔA) vs. wavelength (nm) plot in the near infrared (NIR) range (800–1600 nm) at different time delays is shown for **c** GaN template, **d** Glass/Bi₂Se₃ heterojunction and **e** n-GaN/Bi₂Se₃ heterojunction.

Table 2. Parameters derived from the Glass/Bi₂Se₃ and n-GaN/Bi₂Se₃ transient absorption (TA) spectra and global fitting for lifetime estimation.

Glass/Bi ₂ Se ₃ Film					n-GaN/Bi ₂ Se ₃ Heterojunction				
S.N.	Wavelength (λ) (nm)	$E(\text{eV}) = 1240/\lambda$	$\tau_1(\text{ps})$	$\tau_2(\text{ps})$	$\tau_3(\text{ps})$	Wavelength (λ) (nm)	$E(\text{eV}) = 1240/\lambda$	$\tau_1(\text{ps})$	$\tau_2(\text{ps})$
1	760 (GSB) ¹	1.6	0.78			630 (TA) ²	1.9	150	6990
2	565 (TA) ²	2.2	287	3.4		760 (TA) ³	1.6	248	
3	765 (TA) ³	1.6	2.6	1.08	0.18	765 (GSB) ¹	1.6	1.71	
4	1200 (GSB) ⁴	1.0	5.2			1245 (GSB) ⁴	1.0	6.8	
5	840 (TA) ⁵	1.5	862			825 (TA) ⁵	1.5	540	

GSB and TA reflect the ground state bleaching and transient absorption respectively. Transitions are shown as superscript numeral in correlation with Fig. 3.

gap transitions. At higher wavelengths oscillatory signals were observed due to corrugated structure of GaN substrate. Table 2 and Fig. 3 depict the position of transitions, lifetimes and paths followed on excitation and relaxation.

On excitation with 410 nm pump wavelength in Glass/Bi₂Se₃ film, a ground state bleaching (GSB)^{24,30} appears after 1.28 ps delay in the region of 650–800 nm with maxima ~760 nm (731 fs) for a very short time (parenthesis shows lifetime) for transition 1 (Fig. 2b). GSB is replaced with a transient absorption in the region of 500 nm to 650 nm with maxima ~565 nm for transition 2 (Fig. 3). TA fits with two exponential decay model where the long-lived species shows lifetime of $\tau_1 = 287$ ps. Transient species also appears after 3 ps with maxima ~765 nm for transition 3. In NIR region, broad GSB appears after 1.8 ps delay time with maxima at ~1200 nm with a lifetime of ~5.2 ps (Fig. 2e) for transition 4. TA also appears at 840 nm after ~7 ps of excitation with a lifetime of 862 ps for transition 5.

In the n-GaN/Bi₂Se₃ heterojunction in contrast to Glass/Bi₂Se₃ film, transient absorption appears immediately after 1 ps delay time with ground state bleaching (GSB) at 764 nm (1.71 ps) (Fig. 2c). The transient species appears at 630 nm and 760 nm, and lifetimes are shown in Table 2. Broad GSB band can be seen with maxima ~1245 nm in NIR region (Fig. 2f) for transition 4. Charge

transfer band appears at 630 nm with a very long lifetime of ~7 ns shown as transition 2 in Fig. 3b. GSB appears due to transition of charge carriers from VB to higher CB in both Glass/Bi₂Se₃ films and n-GaN/Bi₂Se₃ heterojunction on pumping with 3.06 eV radiation. However, the lifetime of these transitions is highly different in Bi₂Se₃ film and heterojunctions. In Bi₂Se₃ film, this transition relaxes ultrafast while in heterojunction charge carrier in the excited state are stabilized due to interface effect of Bi₂Se₃ and GaN forming p-n junctions. At the junction electron-hole pair generation is also observed in I-V characteristics of the device at 0V in dark which is discussed in section 2.3. The excited charge carriers stay longer and may involve in other transitions before relaxing back. The long-lived transient species in heterojunction is due to effective charge transfer from GaN to Bi₂Se₃ which further supports the conclusions made by Raman study.

Electrical measurement (I–V) on n-GaN/p-Bi₂Se₃ heterojunction device under dark and illumination conditions

To examine the behavior of the n-GaN/Bi₂Se₃ heterojunction, a schematic in the form of device is constructed (refer. Supplementary Fig. 8a). To examine the real behavior, contacts on either side of the junction have to be ohmic in nature. Aluminum (Al) contact

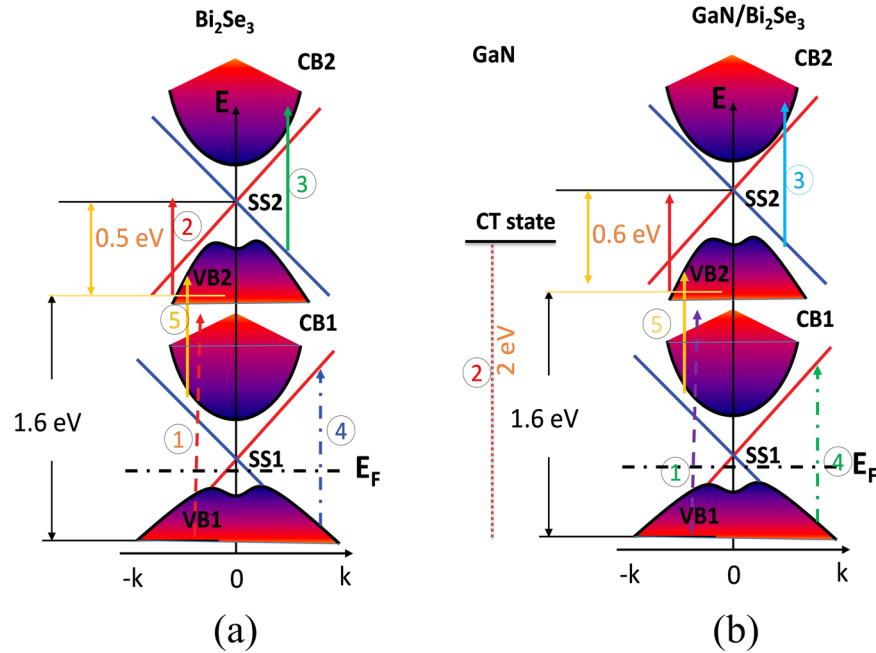


Fig. 3 The energy band structure for the transition of the spin-oriented charge carriers between the different conducting states such as SS1 to SS2, CB1 to SS2, VB1 to SS1, and SS1 to CB2, respectively. **a** Glass/Bi₂Se₃, **b** n-GaN/p-Bi₂Se₃ heterojunction. The SS1, SS2 here represents the two surface states; CB1, CB2 are the first and the second conduction band; VB1, VB2 are the first, and the second valence band. CT here represents the charge transfer state which is present in the n-GaN/p-Bi₂Se₃ heterojunction.

having lesser work function ($W_{Al} = 4.28$ eV) was used as electrode to achieve ohmic contacts with n-GaN semiconductor and low band gap Bi₂Se₃ TI film^{26,31,32}. Ohmic nature of Al-metal contact was further ascertained by measuring I–V characteristics on either side n-GaN/Bi₂Se₃ heterojunction (refer. Supplementary Fig. 9a, b). The I–V results showed rectifying nature with a cut-in voltage of ~ 0.34 V (Fig. 4a, b) due to depletion region formation at the n-GaN and p-Bi₂Se₃ interface (refer. Supplementary Fig. 8b). The p–n diode I–V characteristics across the n-GaN/Bi₂Se₃ heterojunction under the dark conditions is fitted with the ideal diode equation³³ to find various parameters such as ideality factor (n), series resistance and maximum rectification ratio (RR) (refer. Supplementary Section 3 and 4)^{19,20,34}. The ideality factor (n) and series resistance (R_s) was evaluated to be 12.6 and 787 Ω . Other diode parameters are the reverse saturation current (I_R) = 2.22 μ A (at -1 V) and the forward current (I_F) = 621 μ A (at $+1$ V) under dark conditions have good rectifying capacity with maximum rectification ratio (RR) = $(I_F/I_R)_{at \pm 1V} \approx 280$. The high ideality factor ($n=12.6$) in comparison to ideal value (≈ 1) is due to enhanced recombination in depletion region across the heterojunction or due to edge recombination^{35,36} or imperfections in the form of interface states that hints towards CT between GaN and Bi₂Se₃ as we discussed in previous sections. The experimental results of the n-GaN/p-Bi₂Se₃ heterojunction diode under dark were further fitted using the 2-diode simulation model^{37–39}, to extract various diode parameters and found close to the experimental values (refer. Supplementary Section 4 and Fig. 10).

The photoresponse of n-GaN/p-Bi₂Se₃ heterojunction diode was studied under the presence of light by varying the wavelength from 300 nm to 1000 nm at a constant incident light power of 1.96 μ W (Fig. 4a, b). The power was kept low avoiding any possible damage to the surface of the Bi₂Se₃ TI film. The wavelength (λ) of the light was kept in the range from 400 nm to 1000 nm considering the energy bandgap of the two material i.e., the n-GaN (3.4 eV)¹⁵ and p-Bi₂Se₃ (0.3 eV)^{19,20,34}. There can be a hindrance in our results due to the thermoelectric potential which is not desired. This problem is overcome by nullifying the potential across the electrodes by adjusting the incident spot of

light without the applied bias⁴⁰. Under the optical illumination of the light of wavelength (λ) = 300–400 nm an increase in the saturation current (I_R) is observed from the I–V results (Fig. 4b). There is an enhancement in the forward current (I_F) due to the absorption of the light in the n-GaN film having a band gap ($E_g \approx 3.4$ eV) which corresponds to the wavelength (λ) ≤ 365 nm given by the expression $E_g = hc/\lambda = 1.24 \times 10^3/\lambda$ (nm). Here, the Planck's constant (h) = 6.6×10^{-34} J-s, the velocity of light (c) = 3.00×10^8 m/s and E_g is the bandgap in eV, where, 1 eV = 1.6×10^{-19} J. This enhancement in current is also prevalent for a higher range of wavelength till 600 nm wavelength of light (Fig. 4b). However, the saturation or reverse current did not show much increment beyond the 400 nm wavelength, as the charge carrier generated is comparatively lesser due to the least absorption in the n-GaN TI film. From the optical results, we observed that at higher wavelength (λ) ≥ 700 nm of light, current shows a decreasing trend beyond even the dark characteristics which is not the normal trend. This trend is also consistent with higher range of wavelengths of light within the instrument limit. This effect can be correlated with the interfacial effect of the n-GaN/p-Bi₂Se₃ heterojunction which has been seen due to the formation of CT state (Fig. 3b) in the ultrafast study of the charge carrier relaxation. To get deep understanding we need to perform the energy band modeling for the interface behavior of n-GaN/p-Bi₂Se₃ heterojunction device.

Energy band modeling of the n-GaN/p-Bi₂Se₃ heterojunction under dark and illumination

Figure 5 shows the energy band alignment of the n-GaN/p-Bi₂Se₃ heterojunction at thermal equilibrium and forward bias under the dark and the illuminated conditions. E_c , E_v , E_f are the notations used for the respective conduction band, valence band, and Fermi energy level with subscript 1 & 2 denoting n-GaN and p-Bi₂Se₃ material respectively. Figure 5a shows the heterojunction formation with the alignment of the Fermi level and the creation of the space charge region with a built-in potential. ΔE_c , ΔE_v are the valence and the conduction band offset which will form a barrier

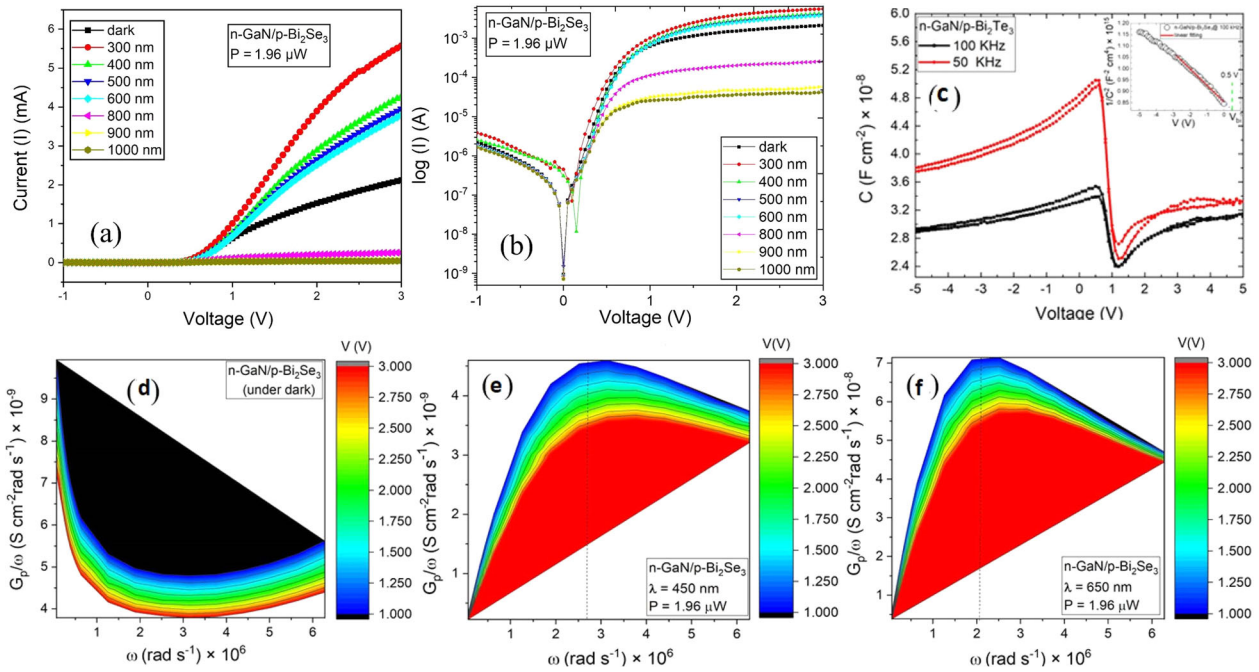


Fig. 4 The current–voltage (I – V), capacitance–voltage (C – V) and conductance/radial frequency (G_p/ω) characteristics are shown for the n-GaN/p-Bi₂Se₃ heterojunction. **a** The I – V plot, **b** semi-log (I – V) plot under dark and illumination conditions with wavelength varied from 300 to 1000 nm at a constant incident light power of 1.96 μ W, **c** C – V plot under dark conditions at constant frequency of 50 and 100 kHz with driving voltage from -1 V to $+3$ V, inset shows the $1/C^2$ – V plot at 100 kHz frequency with x-intercept showing built-in voltage (V_{bi}), **d** G_p/ω – ω plot for voltage biasing from $+1$ V to $+3$ V under dark conditions, **e** G_p/ω – ω plot at $\lambda = 450$ nm, power = 1.96 μ W, **f** G_p/ω – ω plot at $\lambda = 650$ nm, and power = 1.96 μ W.

to the conduction of the electrons from p-Bi₂Se₃ to n-GaN and holes from n-GaN to p-Bi₂Se₃. The theoretical value of ΔE_c , ΔE_v are calculated to be 1.2 eV and 1.9 eV respectively (refer. Supplementary Section 4.2). Under this high barrier of the band offset the only possible conduction is in forward bias as shown through the schematic of the band alignment due to the application of a positive potential to p-Bi₂Se₃ with respect to the n-GaN. Under the thermal equilibrium, there is a small current due to the diffusion of the excess carrier (Fig. 5a) in the form of electrons from n-GaN to p-Bi₂Se₃ and due to the holes from p-Bi₂Se₃ to n-GaN and the formation of the space charge region which balance out the further flow of the charge carriers. This current in the forward biasing is due to the injection of the minority carriers across the junction under the influence of the biasing potential^{34,41}. The forward bias shifts the n-GaN potential and energy bands upwards with respect to p-Bi₂Se₃ and makes it easier for the charge carriers which are electrons and holes (Fig. 5b). The high barrier of the offsets ΔE_c , ΔE_v (1.2 eV and 1.9 eV) did not allow the current in the reverse direction so a very minute negligible current flows in the reverse biasing at room temperature under dark conditions which explain the rectifying behavior of the n-GaN/p-Bi₂Se₃ heterojunction^{41,42}.

Figure 5c shows the forward-biased n-GaN/p-Bi₂Se₃ heterojunction in presence of the light with wavelength (λ). As shown in the schematic of energy bands (Fig. 5c) the incident optical light will generate the charge carrier with the generation of the charge carriers in the form of electrons at the conduction band and holes in the valence band. This generation of charge carriers by the optical light will enhance the current in the n-GaN/p-Bi₂Se₃ heterojunction device as observed from its I – V characteristics (Fig. 4b). The incident photon with wavelength (λ) \leq 365 nm will be absorbed by the n-GaN having bandgap ($E_g \approx 3.4$ eV)¹⁵. Therefore, for the generated charge carriers in n-GaN there is an observed change in the saturation current (I_R) in reverse bias for 300–400 nm of wavelength (Fig. 4b). There is an increase in the

forward current in comparison to the dark conditions due to an increase in charge carrier in the n-GaN/p-Bi₂Se₃ heterojunction as the incident wavelength was varied from 300–600 nm. For wavelength (λ) \geq 700 nm the forward current showed suppression beyond the dark forward current (Fig. 4b). This phenomenon has been attributed to the interface phenomenon of the n-GaN/p-Bi₂Se₃ heterojunction. To study and quantify this interface phenomenon the capacitance-voltage (C – V) measurement for the n-GaN/p-Bi₂Se₃ heterojunction devices were done.

The C – V characteristic of heterojunction is shown in Fig. 4c. No major hysteresis is found when swept with voltage from -1 V to $+3$ V. A shift towards the positive x-axis in the C – V characteristics of the n-GaN/p-Bi₂Se₃ heterojunction is observed revealing the presence of interface states trapped across the junction⁴³. The capacitance is being observed from the C – V characteristics to be enhanced at lower frequency of measurement due to trap states which was able to follow the range of alternating current (AC) frequency and enhances the capacitance value across the heterojunction⁴⁴. The capacitance effect on the biasing becomes less pronounced as we move to high biasing ($V > 2$ V). The carrier concentration of p-Bi₂Se₃ film (N_D) and the built-in potential (V_{bi}) across the junction can be evaluated from the slope and the x-intercept of the $1/C^2$ – V plot⁴⁵ of n-GaN/p-Bi₂Se₃ heterojunction (inset of Fig. 4c) using Eq. 1 as:

$$\frac{1}{C^2} = \frac{2}{q\epsilon A^2 N_D} (V_{bi} - V) \quad (1)$$

The electric permittivity (ϵ) of p-Bi₂Se₃ TI film is given as $\epsilon = 58.25\epsilon_0$ ³⁷ and permittivity of free space (ϵ_0) = 8.85×10^{-12} F/m, the area of the device (A) = 0.0049 cm². The value of N_D and V_{bi} was calculated as 3.37×10^{16} cm⁻³ and 0.5 V from the $1/C^2$ – V plot⁴⁵ and using Eq. 1. The area of our device is lesser than what we have assumed (i.e., 700×700 μ m²) as the diameter of the Aluminum (Al) contact is small (300 μ m) and the fringing current cannot be normalized with that area as the effective area is lesser

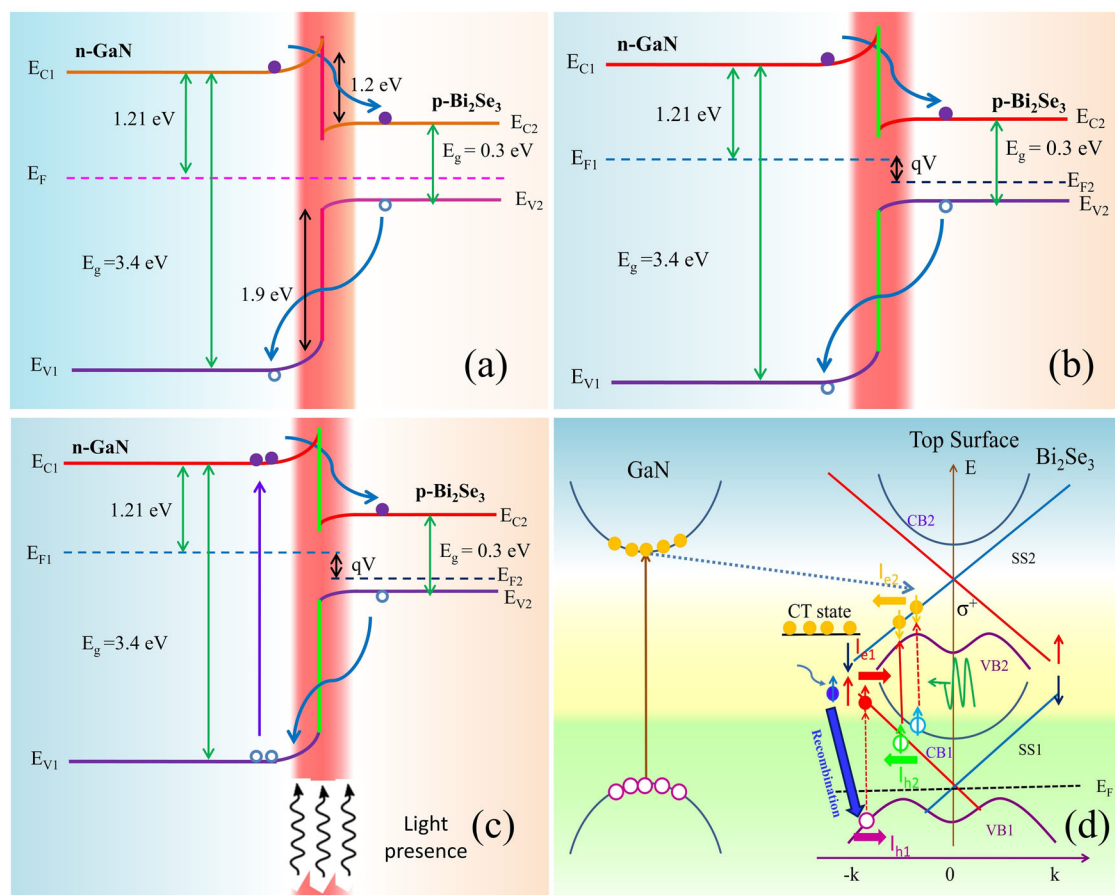


Fig. 5 The schematic of energy band diagram and modelling highlighting the alignment of the band structure of the n-GaN/p-Bi₂Se₃ heterojunction and depletion region (in red). **a** Thermal equilibrium under the dark condition with a built-in voltage and across the junction due to the diffusion of charge carriers, **b** forward bias with the splitting of the Fermi level of the respective material of the heterojunction, **c** forward bias under the influence of light of wavelength (λ) with the generation of the charge carriers and enhancement of current, **d** the surface influence of the Bi₂Se₃ film with the transition of the spin-oriented charge carriers between the SS1 to SS2, CB1 to SS2, and VB1 to SS1, respectively. I_{e1} , I_{h1} represents the photon-induced current due to electrons and the holes at SS1 and VB1. I_{e2} , I_{h2} represent the photon-induced current due to electrons in SS2 and holes in SS1 and CB1.

that the 0.0049 cm^{-2} . It is the reason why the extracted carrier density in Bi₂Se₃ was calculated to be on the lower side ($3.37 \times 10^{16} \text{ cm}^{-3}$) than what we got from the Hall measurement ($N_D = 1.9 \times 10^{18} \text{ cm}^{-3}$). A more accurate effective area can be derived using the numerical simulation for the calculation of the effective area of our device. This discrepancy in the number of charge carriers in p-Bi₂Se₃ film is due to interface defects or barrier in homogeneities⁴⁶ which can be observed by the positive shift of the C–V plot (Fig. 4c).

To get deeper understanding of the behavior and interface density trap⁴⁴, frequency (f) dependence conductance (G_p) measurement was done. Figure 4d–f, show G_p/ω vs. radial frequency ($\omega = 2\pi f$) plot for heterojunction device under dark and illumination showing almost linear decreasing relation with minimum trap density as highlighted from the minima peak in Fig. 4d. The interface traps were not evident in the dark conditions especially at a higher voltage where the trap density was observed to be minimum. At higher frequency (ω) the trap density has the minimum effect on the frequency as the trap states are not able to follow the high AC frequency⁴⁴. The interface peak traps show negligible dependence on the biasing of the heterojunction under the influence of light. The interface traps here, however, showed a little shift towards lower frequency as we move towards the higher wavelength range. At the higher wavelength, the absorption is mostly due to p-Bi₂Se₃ TI film. This trap follows the AC signal of lower frequency^{44,47}. The peaks however have a

Table 3. The calculated value of the density of states (N_{SS}) and the time constant (τ) for the n-GaN/p-Bi₂Se₃ under the presence of light.

Condition	N_{SS} ($\text{eV}^{-1} \text{ cm}^{-2}$)	τ (μs)
Dark	7.2×10^8	~ 10
450 nm	3.5×10^9	~ 0.4
650 nm	5.4×10^9	~ 0.5

minimum effect on the biasing of n-GaN/p-Bi₂Se₃ heterojunction. The value of these interface states (N_{SS}) and the time constant (τ) can be calculated from the $G_p/\omega - \omega$ plot⁴⁴ using the Eq. 2 as: -

$$\frac{G_p}{\omega} = \frac{qN_{SS}}{2\omega\tau} \ln[1 + (\omega\tau)^2] \quad (2)$$

The density of state (N_{SS}) can be calculated from the maxima of the first derivative of Eq. 2 which is: -

$$N_{SS} = \frac{2.5}{q} \left(\frac{G_p}{\omega} \right)_{\max} \quad (3)$$

The values of interface state (N_{SS}) are calculated using Eq. 3 and the time constant (τ) of the interface traps are evaluated by fitting the data (refer. Supplementary Fig. 11). All the evaluated parameters are listed in Table 3 below. As observed from the

Table 3, the density of interface states (N_{SS}) was of the order of 10^8 – 10^9 $\text{eV}^{-1} \text{cm}^{-2}$ and the time constant (τ) ~ 0.5 – 10 μs . The time constant (τ) of the interface traps under the dark is found to be almost double for n-GaN/p-Bi₂Se₃ heterojunction as compared with the presence of light. This interface phenomenon of n-GaN/p-Bi₂Se₃ heterojunction has a charge trapped state at ~ 2 eV (Fig. 5d), as observed in the band diagram of the top surface of the Bi₂Se₃ film, corresponding to the wavelength (λ) = 620 nm of the light as also observed in TA study. Therefore, the wavelength of the light beyond 620 nm i.e., 700–1000 nm shows a suppressed current in comparison to the dark forward current (Fig. 3).

It was not usual for a current to have suppressed forward current beyond a particular wavelength as observed for the n-GaN/p-Bi₂Se₃ heterojunction. This result was consistent for an even range of wavelength beyond 700 nm within the instrument limit. This anomaly in the behavior of the n-GaN/p-Bi₂Se₃ heterojunction is tried to be modeled in the form of the top Dirac cone surface states (Fig. 5d) and its transport properties is studied. Under the presence of the optical light and forward biasing across the n-GaN/p-Bi₂Se₃ heterojunction the spin-polarized charge carriers in n-GaN inject into the neighboring p-Bi₂Se₃ (Fig. 5d). As the holes have stronger relaxation⁴⁸ and lower mobility⁴⁹ in comparison to the electrons, therefore, the current is mainly due to the spin injection of the photo-induced electrons. Under the excitation of the n-GaN/p-Bi₂Se₃ heterojunction with wavelength (λ) ≤ 700 nm, transition from the first surface states (SS1) to the second surface states (SS2), the transition from the first conduction band (CB1) to the second surface state (SS2), and that from the first valence band (VB1) to the SS1, VB1 to VB2 and charge transfer from CB of GaN to CB of Bi₂Se₃ forming CT state are possible⁴⁸. The Dirac point of SS2 is located above the Dirac point of SS1^{48,50–55}. The spin-polarized electrons in n-GaN will inject into p-Bi₂Se₃ film, and injected spin-up electrons will recombine with holes in the VB1. Thereby reducing the holes contribution from the total current particularly at the bottom of the film due to n-GaN substrate. Since, the current we observe is due to combination of current of top and bottom surface current denoted here by I_{e1} and I_{e2} . The suppression of current at bottom surface will enhance the contribution of surface of p-Bi₂Se₃ film in total current⁴⁹. Therefore, a larger current here is observed for wavelength (λ) up to 700 nm. As we move towards a higher wavelength from 700–1000 nm there will be lesser injected electrons from the n-GaN to the p-Bi₂Se₃ as compared to the wavelength (λ) ≤ 700 nm. The other factor is the visible interface CT state which is been shown in p-Bi₂Se₃ film energy structure having energy = 2 eV which corresponds to the wavelength (λ) of 620 nm. Therefore, the charge carriers particularly the electrons cross the barrier of 2 eV when being incident with the wavelength (λ) ≤ 600 nm of the photon light. However, for wavelength (λ) ≥ 700 nm the CT will trap the electrons and reduces the charge carriers and the total flow of the current in the n-GaN/p-Bi₂Se₃ heterojunction device circuit.

To understand the behavior of the photogenerated carrier dynamics, we have performed ultrafast femtosecond transient absorption spectroscopy of Bi₂Se₃ topological insulator film grown on glass substrates and n-GaN substrate. Ground state bleach due to transition of the charge carriers from valence to conduction band and transient absorptions are recorded for both the Bi₂Se₃ film and GaN/Bi₂Se₃ heterojunction on pumping with 3.06 eV radiation probed in visible and NIR regions. Substantial effect on lifetime of these transitions is observed in heterojunction structure. In Bi₂Se₃ films, these transitions relax ultrafast while, in GaN-heterojunction charge carriers in the excited state are stabilized due to interface effect of GaN/Bi₂Se₃ forming p-n junctions. A clear charge-transfer state formation is observed in TA spectra. The generated electron-hole pair is observed in the I - V results at 0 V, which stayed longer and involve in other transitions before relaxing back. The long-lived transient species in

heterojunction is due to effective charge transfer from GaN to Bi₂Se₃ and well supported by the Raman study. Low frequency shift in GaN/Bi₂Se₃ heterostructure implicates GaN effect on the bonding force of Bi₂Se₃ due to electron-phonon coupling. The increased $I(A_{1g}^2)/I(E_g^2)$ in GaAs/Bi₂Se₃ heterojunction confirmed the weaker interaction between the layers. A deeper understanding was established by studying the electrical parameters of n-GaN/p-Bi₂Se₃ heterojunction diode under dark and illuminated conditions. The capacitance-voltage measurement of the n-GaN/p-Bi₂Se₃ diode quantized the number of the interface traps and their time constant and given an understanding of their behavior. The study is significant from the perspective of understanding the modulation of surface states at room temperature in GaN-topological insulator-based interface device showing their potential towards next-generation electronic and optical devices.

METHODS

Experimental details

The n-GaN film of thickness ~ 3.5 μm grown over a c-plane sapphire (S) having a thickness of ~ 0.33 mm was employed as a substrate to fabricate Bi₂Se₃ TI heterojunctions. For n-GaN/p-Bi₂Se₃ heterojunction fabrication, substrate was loaded in thermal coating unit (Scientific & Analytical Instruments). A powdered Bi₂Se₃ precursor of a purity $\sim 99.98\%$ (on the metal basis) was used to grow a thin TI film on n-GaN substrates. Bi₂Se₃ TI film of same thickness was also grown on glass substrate for reference. Thickness was controlled by Quartz crystal monitor in vacuum chamber and also confirmed by ellipsometer (J. A. Wollam co. Inc., United States). The grown Bi₂Se₃ TI film was annealing temperature of 200 °C for 2 h in the presence of the Argon (Ar) gas. The crystal planes of Bi₂Se₃ TI films were identified by X-ray diffractometer (XRD) (Rigaku Miniflex, model no. BD68000014-01). Microstructure and morphology study were done by scanning electron microscopy (SEM-EDS) (Model No. EVO 15, ZEISS EVO Series) and atomic force microscopy (AFM) (Agilent Technologies, Model: 5500). Raman spectroscopy was used to study the active modes. The Raman characterization was done with 534 nm laser light with the and scattering was with the lowest Raman shift of 10 cm^{-1} . Pump-probe spectroscopy was used to probe the transient dynamics of charge carriers of the Bi₂Se₃ TI film grown on glass and n-GaN substrates. The Titanium (Ti): Sapphire laser amplifier with specifications: 35 fs, 4 mJ/pulse, 1 kHz, 800 nm) was used with two fragments of light. 410 nm pump wavelength was used and probe was varied from visible (VB) to near-infrared (NIR) range (400–1600 nm) at 7 fs time delay with pump. The pump power was kept low at 35 μW to make it a non-destructive process and preserving the film from any possible damage. n-GaN/Bi₂Se₃ heterojunctions device was realized by growing metallic contacts across the junction. Aluminum wire with a purity of $\sim 99.999\%$ was used to grow metallic contacts by thermal evaporation technique under a high vacuum (10^{-6} Torr). The metal contacts were grown through the metallic shadow mask with dimensions: diameters ~ 300 μm and inter distance ~ 600 μm . The metal contact across the n-GaN/Bi₂Se₃ heterojunction of thickness ~ 150 nm was confirmed by the ellipsometer. The nearest contacts across the n-GaN/Bi₂Se₃ heterojunction were used as 2-probes for electrical characterization (Keithley 4200SCS). A tunable light source (NewPort TLS 300XU) with varying wavelengths (300–1000 nm) was used to illuminate light across these nearest contacts across the n-GaN/Bi₂Se₃ heterojunction. Semi-Probe station was used for all the current-voltage (I - V), capacitance-voltage (C - V), and capacitance-frequency (C - f) and optical characterization through two 4, 225 RPM/SMU. The details fabrication process of the n-GaN/p-Bi₂Se₃ heterojunction diode is discussed in details in the Supplementary material (Section 1) and also with the fabrication flow process (Supplementary Fig. 1). Details can also be found in our previous works^{19,20,22,34}.

DATA AVAILABILITY

All data generated or analyzed during this study are included in this published article (and its supplementary information files).

Received: 17 August 2021; Accepted: 20 January 2022;
Published online: 28 February 2022

REFERENCES

- Politano, A., Viti, L. & Vitiello, M. S. Optoelectronic devices, plasmonics, and photonics with topological insulators. *APL Mater.* **5**, 35504 (2017).
- Tian, W., Yu, W., Shi, J. & Wang, Y. The property, preparation and application of topological insulators: a review. *Mater. (Basel)* **10**, 814 (2017).
- Hor, Y. S., Chechelsky, J. G., Qu, D., Ong, N. P. & Cava, R. J. Superconductivity and non-metallicity induced by doping the topological insulators Bi_2Se_3 and Bi_2Te_3 . *J. Phys. Chem. Solids* **72**, 572–576 (2011).
- Ambrosi, A., Sofer, Z., Luxa, J. & Pumera, M. Exfoliation of layered topological insulators Bi_2Se_3 and Bi_2Te_3 via electrochemistry. *ACS Nano* **10**, 11442–11448 (2016).
- Zhang, F., Kane, C. L. & Mele, E. J. Surface states of topological insulators. *Phys. Rev. B* **86**, 81303 (2012).
- Zhang, T. et al. Experimental demonstration of topological surface states protected by time-reversal symmetry. *Phys. Rev. Lett.* **103**, 266803 (2009).
- Wang, J. et al. Evidence for electron-electron interaction in topological insulator thin films. *Phys. Rev. B* **83**, 245438 (2011).
- Jiang, Y. et al. Landau quantization and the thickness limit of topological insulator thin films of Sb_2Te_3 . *Phys. Rev. Lett.* **108**, 16401 (2012).
- Haim, A., Ilan, R. & Alicea, J. Quantum anomalous parity Hall effect in magnetically disordered topological insulator films. *Phys. Rev. Lett.* **123**, 46801 (2019).
- Wiesner, M. et al. The effect of substrate and surface plasmons on symmetry breaking at the substrate interface of the topological insulator Bi_2Te_3 . *Sci. Rep.* **9**, 1–8 (2019).
- Backes, D. et al. Disentangling surface and bulk transport in topological-insulator p–n junctions. *Phys. Rev. B* **96**, 125125 (2017).
- Steinberg, H., Laloë, J. B., Fatemi, V., Moodera, J. S. & Jarillo-Herrero, P. Electrically tunable surface-to-bulk coherent coupling in topological insulator thin films. *Phys. Rev. B* **84**, 233101 (2011).
- Chae, J. et al. Closing the surface bandgap in thin Bi_2Se_3 /graphene heterostructures. *ACS Nano* **13**, 3931–3939 (2019).
- Zeng, Z. et al. Broadband detection based on 2D Bi_2Se_3 /ZnO nanowire heterojunction. *Crystals* **11**, 169 (2021).
- Turut, A., Doğan, H. & Yıldırım, N. The interface state density characterization by temperature-dependent capacitance–conductance–frequency measurements in Au/Ni/n-GaN structures. *Mater. Res. Express* **2**, 96304 (2015).
- Zhang, H., Zhang, X., Liu, C., Lee, S. T. & Jie, J. High-responsivity, high-detectivity, ultrafast topological insulator Bi_2Se_3 /silicon heterostructure broadband photodetectors. *ACS Nano* **10**, 5113–5122 (2016).
- Sánchez-Barriga, J. et al. Nonmagnetic band gap at the Dirac point of the magnetic topological insulator $(\text{Bi}_{1-x}\text{Mn}_x)_2\text{Se}_3$. *Nat. Commun.* **7**, 1–10 (2016).
- Takahashi, R. & Murakami, S. Thermoelectric transport in topological insulators. *Semicond. Sci. Technol.* **27**, 124005 (2012).
- Ahmad, F., Kandpal, K. & Kumar, P. Electrical properties of a metal-germanium-topological insulator (metal/n-Ge/p- Bi_2Te_3) heterostructure devices. *J. Mater. Sci. Mater. Electron.* **32**, 8106–8121 (2021).
- Ahmad, F. et al. Fabrication of a p–n Heterojunction using topological insulator Bi_2Te_3 -Si and its annealing response. *J. Electron. Mater.* **47**, 6972–6983 (2018).
- Kumar, P. et al. Anomalous magnetoresistance in topological insulator Bi_2Te_3 . *Adv. Mater. Proc.* **1**, 21–21 (2016).
- Maurya, G. K. et al. Dual-quadrant photodetection in topological insulator and silicon-based heterojunction (n- Bi_2Te_3 /p-Si). *Appl. Surf. Sci.* **565**, 150497 (2021).
- Jnawali, G. et al. Revealing optical transitions and carrier recombination dynamics within the bulk band structure of Bi_2Se_3 . *Nano Lett.* **18**, 5875–5884 (2018).
- Glinka, Y. D., Li, J., He, T. & Sun, X. W. Clarifying ultrafast carrier dynamics in ultrathin films of the topological insulator Bi_2Se_3 using transient absorption spectroscopy. *ACS Photonics* **8**, 1191–1205 (2021).
- Liu, X. et al. Characterization of Bi_2Te_3 and Bi_2Se_3 topological insulators grown by MBE on (001) GaAs substrates. *J. Vac. Sci. Technol. B, Nanotechnol. Microelectron. Mater. Process. Meas. Phenom.* **30**, 02B103 (2012).
- Gupta, G., Jalil, M. B. A. & Liang, G. Evaluation of mobility in thin Bi_2Se_3 topological insulator for prospects of local electrical interconnects. *Sci. Rep.* **4**, 1–6 (2014).
- Tongay, S. et al. Tuning interlayer coupling in large-area heterostructures with CVD-grown MoS_2 and WS_2 monolayers. *Nano Lett.* **14**, 3185–3190 (2014).
- Potter, A. C., Kimchi, I. & Vishwanath, A. Quantum oscillations from surface Fermi arcs in Weyl and Dirac semimetals. *Nat. Commun.* **5**, 1–6 (2014).
- Zhang, Y. & Vishwanath, A. Anomalous Aharonov-Bohm conductance oscillations from topological insulator surface states. *Phys. Rev. Lett.* **105**, 206601 (2010).
- Yang, X. et al. Light control of surface–bulk coupling by terahertz vibrational coherence in a topological insulator. *npj Quantum Mater.* **5**, 1–7 (2020).
- Liu, Y. Recent research on ohmic contacts on GaN-based materials. In *IOP Conference Series: Materials Science and Engineering* 738, 12007 (IOP Publishing, 2020).
- Wang, Z. et al. Tuning carrier type and density in Bi_2Se_3 by Ca-doping. *Appl. Phys. Lett.* **97**, 42112 (2010).
- Sze, S. M., Li, Y. & Ng, K. K. *Physics of semiconductor devices*. (John Wiley & sons, 2021).
- Ahmad, F., Kandpal, K., Kumar, N., Kumar, R. & Kumar, P. Effect of different metallic contacts on the device performance of a p–n heterostructure of a topological insulator and silicon (p- Bi_2Te_3 /n-Si). *IEEE Trans. Electron Devices* **67**, 5388–5395 (2020).
- Decock, K., Khelifi, S. & Burgelman, M. Modelling multivalent defects in thin film solar cells. *Thin Solid Films* **519**, 7481–7484 (2011).
- Ajimsha, R. S. et al. Transparent p-AgCoO₂/n-ZnO diode heterojunction fabricated by pulsed laser deposition. *Thin Solid Films* **515**, 7352–7356 (2007).
- Project, T. M. Materials Data on Bi_2Se_3 by Materials Project. (2017). <https://doi.org/10.17188/1266263>
- Breitenstein, O. & Riñland, S. A two-diode model regarding the distributed series resistance. *Sol. Energy Mater. Sol. Cells* **110**, 77–86 (2013).
- McIntosh, K. R. Lumps, humps and bumps: three detrimental effects in the current–voltage curve of silicon solar cells. In: *Centre for Photovoltaic Engineering*. (Univ. New South Wales, Aust., 2001).
- Zhang, H. et al. Anomalous photoelectric effect of a polycrystalline topological insulator film. *Sci. Rep.* **4**, 1–5 (2014).
- Sze, S. M. & Ng, K. K. *Physics of semiconductor devices*. (John Wiley & sons, 2006).
- Kumar, R. et al. Flexible perylenedimide/GaN organic–inorganic hybrid system with exciting optical and interfacial properties. *Sci. Rep.* **10**, 1–11 (2020).
- Sze, S. M. *Semiconductor devices: physics and technology*. (John Wiley & sons, 2008).
- Shi, Y. et al. Investigation of bulk traps by conductance method in the deep depletion region of the Al_2O_3 /GaN MOS device. *Nanoscale Res. Lett.* **12**, 1–6 (2017).
- Cristea, M. J. Capacitance-voltage profiling techniques for characterization of semiconductor materials and devices (2019). Available at SSRN: <https://doi.org/10.2139/ssrn.3433675>.
- Hussain, I., Soomro, M. Y., Bano, N., Nur, O. & Willander, M. Interface trap characterization and electrical properties of Au-ZnO nanorod Schottky diodes by conductance and capacitance methods. *J. Appl. Phys.* **112**, 64506 (2012).
- Kandpal, K., Gupta, N., Singh, J. & Shekhar, C. Study of ZnO/BST interface for thin-film transistor (TFT) applications. *Surf. Interfaces* **23**, 100996 (2021).
- Tu, C.-M. et al. Manifestation of a second Dirac surface state and bulk bands in THz radiation from topological insulators. *Sci. Rep.* **5**, 1–8 (2015).
- Yu, J. et al. Control of circular photogalvanic effect of surface states in the topological insulator Bi_2Te_3 via spin injection. *ACS Appl. Mater. Interfaces* **12**, 18091–18100 (2020).
- Wang, M. C., Qiao, S., Jiang, Z., Luo, S. N. & Qi, J. Unraveling photoinduced spin dynamics in the topological insulator Bi_2Te_3 . *Phys. Rev. Lett.* **116**, 36601 (2016).
- Huang, Y. Q., Song, Y. X., Wang, S. M., Buyanova, I. A. & Chen, W. M. Spin injection and helicity control of surface spin photocurrent in a three dimensional topological insulator. *Nat. Commun.* **8**, 15401 (2017).
- Kung, H. H. et al. Observation of chiral surface excitons in a topological insulator Bi_2Se_3 . *Proc. Natl Acad. Sci. USA* **116**, 4006–4011 (2019).
- Sobota, J. A. et al. Direct optical coupling to an unoccupied Dirac surface state in the topological insulator Bi_2Se_3 . *Phys. Rev. Lett.* **111**, 136802 (2013).
- Soifer, H. et al. Band-resolved imaging of photocurrent in a topological insulator. *Phys. Rev. Lett.* **122**, 167401 (2019).
- Fernandes, W. P., de Siervo, A. & Soares, E. A. Photoelectron diffraction study of the Bi_2Se_3 (0001) surface. *MRS meeting; Campinas, SP (Brazil)*, **49**, 15 (2016).

ACKNOWLEDGEMENTS

The authors would like to thank DST, Govt. of India for providing the financial support to carry out this work. VLSI Lab, Department of Electronics and communications, IIIT Allahabad for electrical characterization. CIR, MNNIT-Allahabad for providing the material characterization facilities. My colleague Mr. Sanjay Sharma and Mr. Gyanendra Maurya, Spintronics and Magnetic Materials Laboratory, IIIT Allahabad, for helping me with the technical drawing of the device schematic and the energy band structures.

AUTHOR CONTRIBUTIONS

P.K., F.A. and R.K. conceived the initial research idea and planned the study. P.K. and F.A. did the electrical analysis. R.K. and P.K. did the Raman and transient absorption analysis. F.A., P.K. and R.K. wrote the manuscript. S.S. provided the GaN substrate and Raman data. M.K. recorded the ultra-fast transient absorption data.

COMPETING INTERESTS

The authors declare no competing interests.

ADDITIONAL INFORMATION

Supplementary information The online version contains supplementary material available at <https://doi.org/10.1038/s41699-022-00288-7>.

Correspondence and requests for materials should be addressed to Rachana Kumar or Pramod Kumar.

Reprints and permission information is available at <http://www.nature.com/reprints>

Publisher's note Springer Nature remains neutral with regard to jurisdictional claims in published maps and institutional affiliations.



Open Access This article is licensed under a Creative Commons Attribution 4.0 International License, which permits use, sharing, adaptation, distribution and reproduction in any medium or format, as long as you give appropriate credit to the original author(s) and the source, provide a link to the Creative Commons license, and indicate if changes were made. The images or other third party material in this article are included in the article's Creative Commons license, unless indicated otherwise in a credit line to the material. If material is not included in the article's Creative Commons license and your intended use is not permitted by statutory regulation or exceeds the permitted use, you will need to obtain permission directly from the copyright holder. To view a copy of this license, visit <http://creativecommons.org/licenses/by/4.0/>.

© The Author(s) 2022